OXFORD

Journal of Geophysics and Engineering

Journal of Geophysics and Engineering (2023) **20**, 78–90 https://doi.org/10.1093/jge/gxac097

Petrophysical characteristics and identification parameters of the Jurassic continental shale oil reservoirs in the Central Sichuan Basin

Yichen Song [1,2,†], **Lianbo Zeng** [1,2,*], **Fei Gong** [3,2], **Ping Huang** [4], **Wenya Lyu** [1,2] **and Shaoqun Dong** [1,2]

[1] State Key Laboratory of Petroleum Resources and Prospecting, China University of Petroleum (Beijing), Beijing, 102249, China
[2] College of Geosciences, China University of Petroleum (Beijing), Beijing, 102249, China
[3] College of Geoscience and Surveying Engineering, China University of Mining and Technology (Beijing), Beijing, 100086, China
[4] Research Institute of CNPC Southwest Oil and Gas Field Branch, Chengdu, 641500, China

*Corresponding author: Lianbo Zeng. E-mail: lbzeng@sina.com

†First Author: Yichen Song. E-mail: 2017011242@student.cup.edu.cn

Received 17 July 2022, revised 20 November 2022
Accepted for publication 12 December 2022

Abstract

The Sichuan Basin in south-western China is rich in shale oil in the Jurassic strata. Due to its complex geological characteristics, reservoir identification using current log-constrained seismic inversion methods is difficult. Characteristics of the shale oil reservoirs were tested on the basis of the petrophysical experimentation of core samples from the said strata. Thin sections and logging data analysis showed the influencing factors on petrophysical characteristics and clarified the sensitive geophysical parameters for reservoir identification. The Da'anzhai Member reservoirs were determined to have high acoustic velocities, V_p/V_s ratios and Young's moduli, and low Poisson's ratios. Several geological factors have influenced the petrophysical properties of the reservoirs. The Da'anzhai Member reservoirs are characterized by a low content of clay minerals and the development of fractures and laminae. The presence of clay minerals caused general high acoustic velocities of the reservoirs; the presence of fractures and laminae in high-quality reservoirs results in a decrease of the acoustic velocities. Therefore, the relatively low value against the background of high acoustic velocity can be used as the criteria for high-quality reservoirs. Poisson's ratio is obviously different in reservoirs and non-reservoirs. When it is <0.269, the reservoirs can be fully identified. In addition, the combination of the Lame constant and shear modulus ($\lambda > 25.277$ and $\mu > 20.72$ GPa), P-wave and S-wave velocity ($V_p > 4967$ and $V_s > 2781$ m s^{-1}), wave impedance and V_p/V_s ratio (AI > 13.319 g · cm^3 · km · s^{-1} and $V_p/V_s > 1.792$) can also provide references for reservoir identification.

Keywords: petrophysical characteristics, continental shale oil, reservoir identification, Central Sichuan Basin

1. Introduction

The Sichuan Basin, the main petroliferous area in southwest China, is featured in rich reservoirs of Jurassic continental shale oil (Yang *et al.* 2016). However, it is a challenge to apply the log-constrained seismic inversion method for reservoir identification and prediction in this area due to the complex sedimentary conditions, thinly interbedded reservoirs and widespread tectonic fractures, which significantly limit the exploration of continental shale oil (Gan *et al.* 2009; Zeng *et al.* 2016; Tian *et al.* 2021). The rock physical property, which connects the seismic data, well logs and reservoir parameters, forms the basis for geophysical reservoir identification and prediction (Sun *et al.* 2021). Therefore, research about essential petrophysical properties of the Jurassic shale oil reservoirs in the Sichuan Basin is significant for exploring continental shale oil.

In the Sichuan Basin, discovered shale oil reservoirs are mainly distributed in the Shaximiao Formation (J_2S), Da'anzhai Member (J_1dn) and Liangshan Formation (J_2l). The Da'anzhai Member is the primary petroliferous strata, comprising shell limestone, shale, and mudstone (Pang *et al.* 2018, 2020). The shale is the main source rock and play a dominant role in both single layer thickness and cumulative proportion. The shell limestone is the main reservoir intervals, frequently interbedded with shale intervals, which constitutes a set of hydrocarbons bearing layers dominated by shale (Chen *et al.* 2015; Li *et al.* 2020). Microscopically, the pore throat radius of the reservoirs is small with poor sorting, forming a complex pore throat structure. The intrusive mercury curve shows that the displacement pressure of pores is high (Li *et al.* 2020). The porosity is less than 1%, and the permeability is less than 0.5 mD (Su *et al.* 2020, Tian *et al.* 2021), characterized by ultralow porosity and ultralow permeability. Micro/nanopores dominate the reservoir spaces, pores with a diameter of >1 μm are mostly micro-fractures and dissolution pores (Tian *et al.* 2017) and pores <1 μm are mainly intragranular and intergranular pores (Xu *et al.* 2019). The reservoirs have a dual pore-fracture space type (Pang *et al.* 2018, 2020). As the main reservoir spaces and migration pathways, fractures directly influence the oil and gas production efficiency (Zeng *et al.* 2009, Ding *et al.* 2016, 2016, Gong *et al.* 2021a). Under the medium-deep burial diagenetic environment, the complex tectonic stress can simultaneously produce fractures of different angles and form dense fracture networks. The reservoirs with widely developed fractures in the Da'anzhai Member generally have better reservoirs and connectivity, which can be considered high-quality reservoirs (Zeng *et al.* 2016; Gong *et al.* 2019, 2021b; Liu *et al.* 2021). Current research focuses on the qualitative geological description of shale oil reservoirs but lacks quantitative analysis of petrophysical characterization.

Most of the reservoir strata in Da'anzhai Member are thin inter-beds, for which the strata distribution characteristics cannot be reflected accurately by conventional seismic reflection parameters. Therefore, a high-resolution inversion technology is a must in this aspect (Liu 2021). Log-constrained seismic inversion is a high-resolution inversion method under the constraints of geological laws (Karimpouli *et al.* 2013). First, the internal relationship between petrophysical parameters and seismic elastic parameters is established through the analysis of petrophysical characteristics. Then the seismic elastic parameters sensitive to the reservoir are selected, which can be used to guide seismic inversion and the interpretation of inversion results and realize the prediction of the distribution of oil and gas reservoir (Aleardi 2018; Liu *et al.* 2019; Gao *et al.* 2021). Scholars have made specific progress in identifying and predicting the Da'anzhai Member reservoirs. Peng *et al.* (2014) quantitatively predicted the reservoirs' distribution by uranium logging and seismic impedance inversion. Tian *et al.* (2017) systematically analysed the relation among matrix pores, fractures, physical properties and oiliness of the Da'anzhai Member and reported that the siliceous and argillaceous shell limestone were potential reservoirs. Pang *et al.* (2020) calibrated the GR logs and the rock types to figure that 'GR $<$ 30 API' is a practical standard for reservoir identification. Tian *et al.* (2021) established the template of resistivity logs, with which the fracture scale, density and filling degree of the Da'anzhai Member reservoirs are predicted effectively. Current studies on predicting reservoirs' distribution are mainly based on the response characteristics of seismic waves and logging curves. The analyses on petrophysical characteristics and sensitivity parameters on cores are still relatively weak. There is a lack of support from dynamic and static petrophysical experiments when using the log-constrained seismic inversion method to predict reservoir distribution.

We analysed the petrophysical characteristics of core samples in the Da'anzhai Member on the basis of ultrasonic pulse-transmission and triaxial rock compression experiments. Combined with thin sections and well logging interpretation, we discussed the main factors influencing the petrophysical characteristics and influencing mechanisms. Finally, we selected sensitive parameters for reservoir identification. The research results can provide essential petrophysical experimental evidence for identifying and predicting the Da'anzhai Member reservoirs based on the log-constrained seismic inversion method.

2. Geological setting

Featured in a multi-directional thrust nappe tectonic background, the Sichuan Basin is a secondary tectonic unit in the north-western part of the Yangtze Plate with a rhombus shape and a clear boundary outline. Figure 1 shows the main tectonic divisions inside and surrounding the basin. It is surrounded by the Longmenshan, Dabashan, Bamianshan,

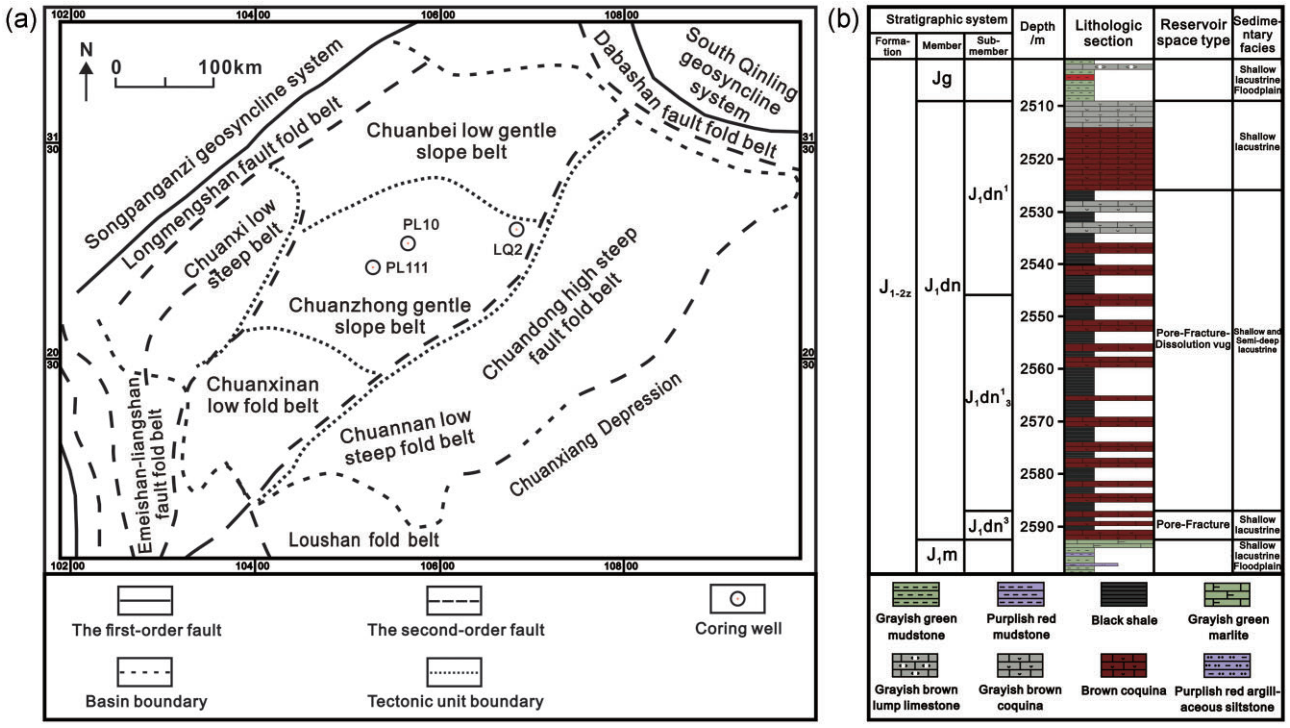

Figure 1. (a) The Geological map of the Central Sichuan Basin (Core well PL10, PL111, LQ2). (b) The comprehensive stratigraphic columnar section of the Da'anzhai Member.

Table 1. Basic information of samples (Xu *et al.* 2018, 2019)

Rock type	Number	Sampling stratum	Density (g/cm^3)	Calite (%)	Quartz (%)	Clay minerals (%)
Shell limestone	17 samples from the reservoir intervals; 6 samples from the non-reservoir intervals	Da'anzhai Member	2.705	60–90	5–25	5–15

Loushan and Emeishan-Liangshan Fault Fold Belts (Li & He 2014). Under multiple stages of tectonic evolution, the tectonic framework of the Sichuan Basin was initially formed during the Indosinian Movement and then further developed during the Yanshan Movement; during the Himalayan Movement period, it was intensely rebuilt and finally presents the geological features now (Li *et al.* 2016; Zeng *et al.* 2022). Due to high thermal maturity, the Jurassic lacustrine source rocks are at the oil generation stage. The oil-producing areas are mainly distributed in the Central Sichuan Basin (Yang *et al.* 2016).

The Central Sichuan Basin stretches to the western Longquanshan Tectonic Belt and the eastern Huayingshan Fault Belt. Being influenced by the uplift of the Huayingshan Fault Belt, the general tectonic terrain of this area dips from east to west in a nose-like shape (Xu *et al.* 2012). Due to the great basement rigidity, this study area is mainly dominated by gentle folds and only a few large-scale faults. However, the diversified tectonic types and features, as well as the tectonic stress changed in multiple directions, make the strata suffer irregular forces, which provide a condition beneficial for forming fractures (Zeng 2010; Li *et al.* 2018). After over 50 years of exploration, Jinhua, Gongshanmiao, Lianchi, Guihua, Zhongtaishan and other 15 hydrocarbon bearing blocks have been found by China National Petroleum Corporation (Chen *et al.* 2015). Da'anzhai Member is the major production layer, wells from Da'anzhai Member are increasing in numbers across the entire Central Sichuan area, thereby providing detailed data support for this research.

The sedimentary thickness of the Jurassic strata is extensive and complete in the Sichuan Basin. Six sets of petroliferous strata are in the Jurassic, including the Shayi Member (J_2S^1), the Liangshan Formation (J_2l), the Da'anzhai Member (J_1dn), the Ma'anshan Member (J_2m), the Dongyuemiao Member (J_1d) and the Zhenzhuchong Member (J_1z) (Yang *et al.* 2016; Wang *et al.* 2018). Figure 1 shows the comprehensive strata histogram of the Da'anzhai Member; it is dominated by brown shell limestone and black

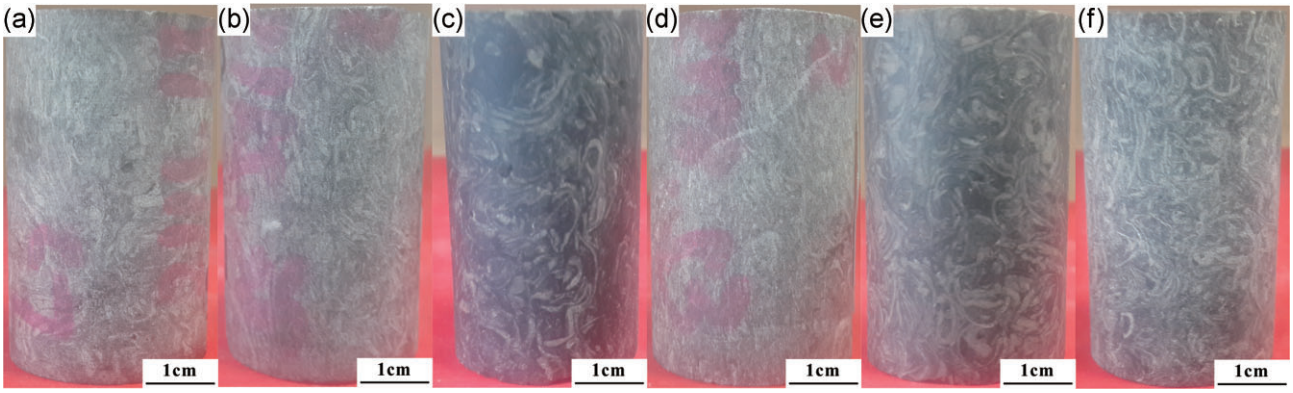

Figure 2. Typical shell limestone samples of the Da'anzhai Member. (a) Reservoir intervals at a depth of 2118.53 m in the Well LQ2. (b) Reservoir intervals at a depth of 2111.36 m in the Well LQ2. (c) Reservoir intervals at a depth of 2135.05 m in the Well PL10. (d) Non-reservoir intervals at a depth of 1981.8 m in the Well PL10. (e) Non-reservoir intervals at a depth of 2115.38 m in the Well LQ2. (f) Non-reservoir intervals at a depth of 2033.13 m in the Well PL10.

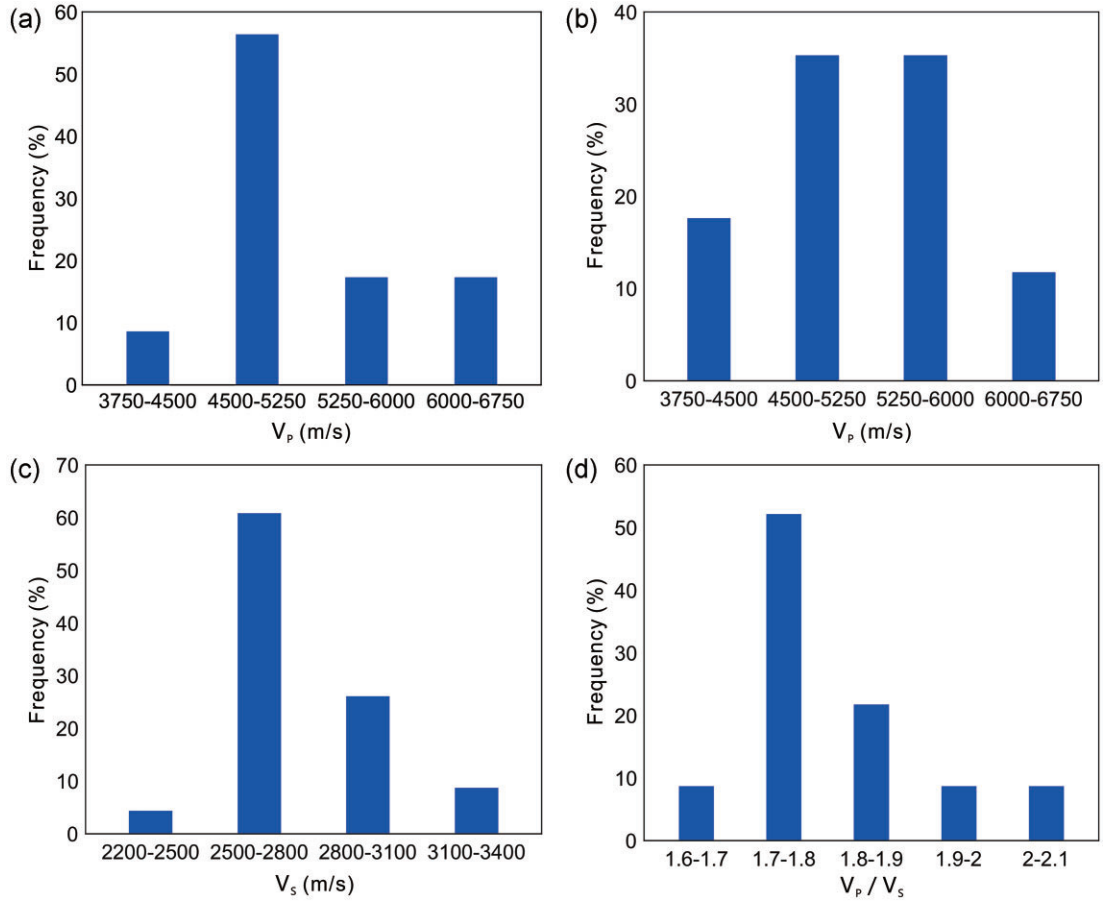

Figure 3. The distribution ranges of (a) P-wave velocities (V_p) from experimental results, (b) P-wave velocities (V_p) from well logging data, (c) S-wave velocities (V_s) and (d) V_p/V_s ratios of the Da'anzhai Member ($N = 23$).

shale (Pang *et al.* 2018, 2020). From the sedimentary evolution profile, the Da'anzhai Member has experienced the complete cycle of sea-level evolution from the expansion period, the peak period, to the contraction period. The corresponding strata are divided into three submembers: the Dayi, Dayisan and Dasan. The Dayi and Dasan submembers are featured in the development of shell limestone with coastal shallow lake facies; the Dayisan submember is featured in the development of shale with shallow and semi-deep lake facies (Chen *et al.* 2015; Yang *et al.* 2017). It can be seen from the plane that the sedimentary facies are distributed in a ring-like shape, which is respectively the semi-deep lake facies, the shallow lake facies and the lakeshore facies from the centre to the edge of the lake basin (Xu *et al.* 2020). The strata are

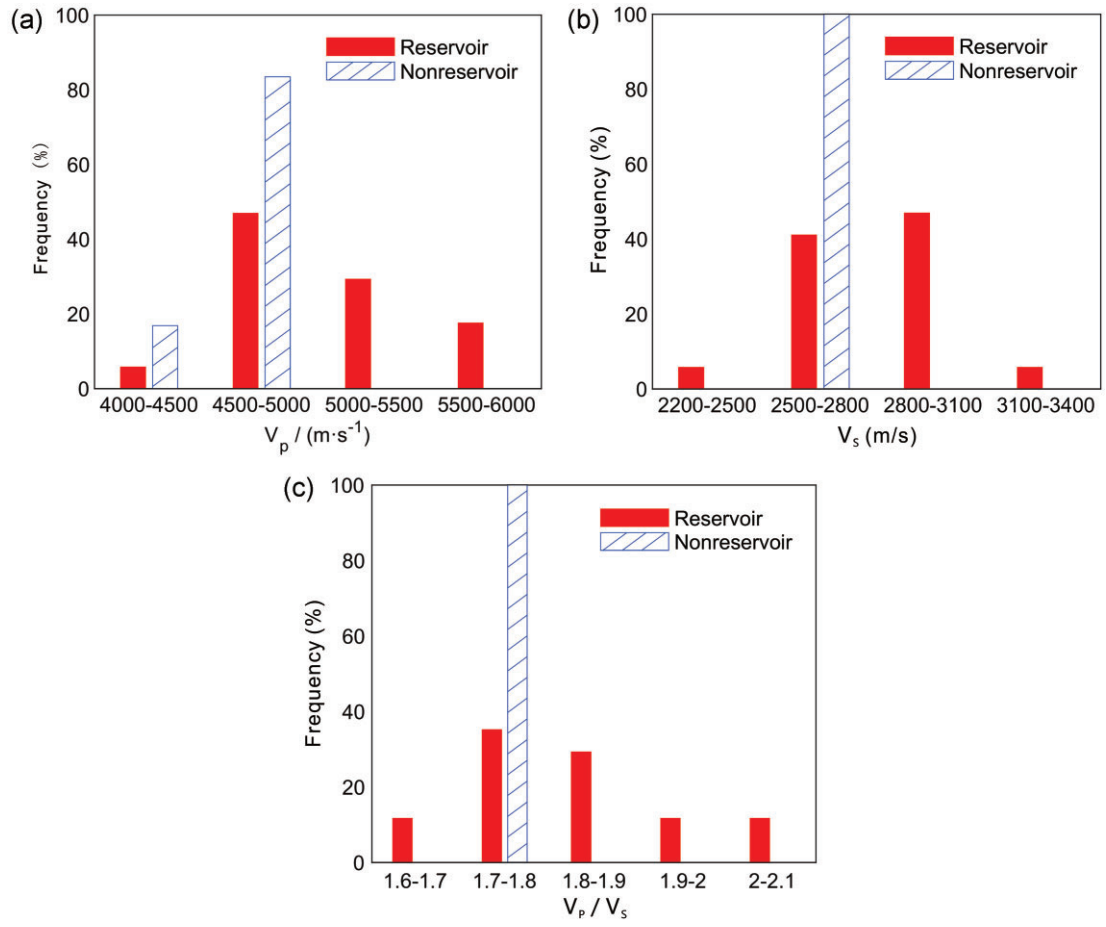

Figure 4. The distribution ranges of (a) P-wave velocities (V_p), (b) S-wave velocities (V_s) and (c) V_p/V_s ratios of the reservoir intervals and the non-reservoir intervals of the Da'anzhai Member ($N = 23$).

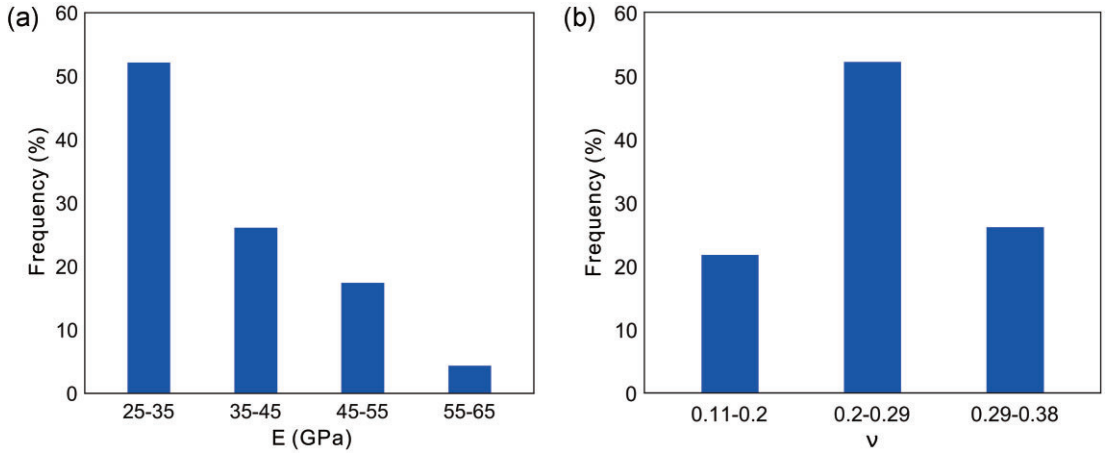

Figure 5. The distribution ranges of (a) Young's moduli (E) and (b) Poisson's ratios (ν) of the Da'anzhai Member ($N = 23$).

2300–2800 m deep and 80–110 m thick, developing black shale with the semi-deep lake facies and shell limestone with the coastal lake biological shell facies (Peng *et al.* 2014).

The primary petroliferous Jurassic strata were distributed continuously on the plane. They were not subject to the control of the tectonic topographies and manifested as unconventional oil and gas accumulations (Xu *et al.* 2017; Zhang & Tang 2022). Among them, the Da'anzhai Member reservoirs rich in oil and gas are distributed mainly in Dayi, Dayisan and Dasan submembers along the vertical direction. Dayisan submember is dominated by shale, which is the main source rock of the Da'anzhai Member; it primarily

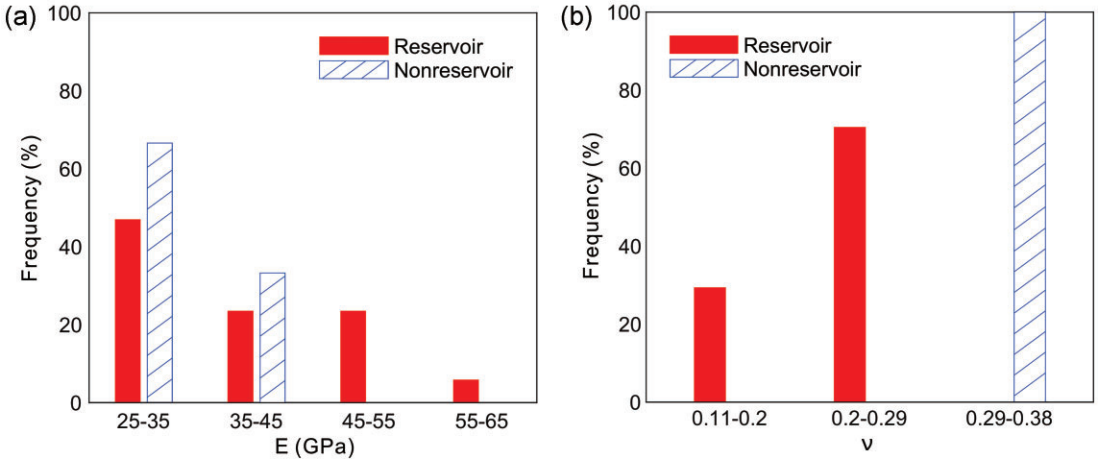

Figure 6. The distribution ranges of (a) Young's moduli (E) and (b) Poisson's ratios (ν) of the reservoir intervals and the non-reservoir intervals of the Da'anzhai Member ($N = 23$).

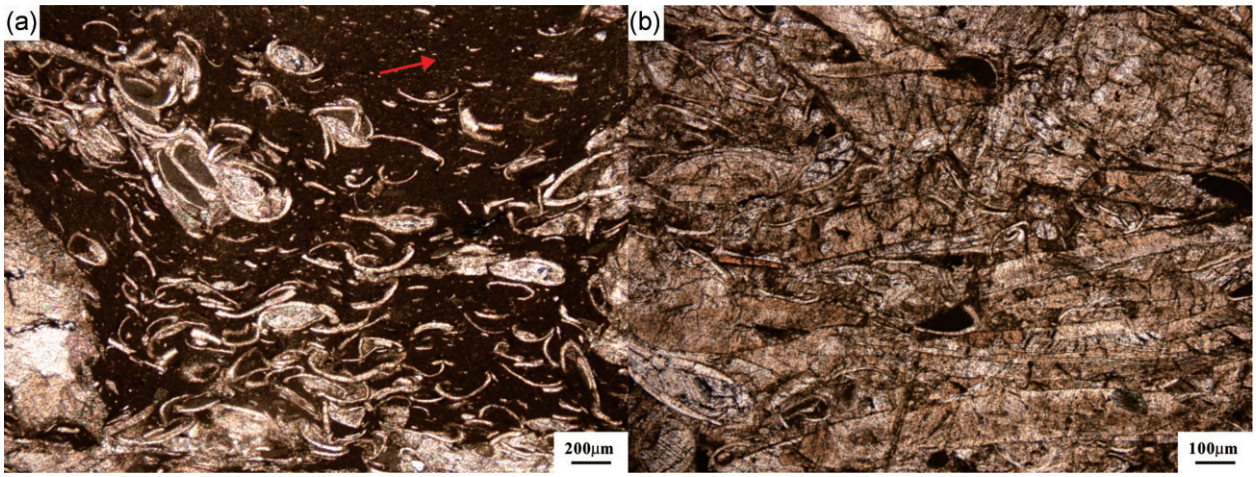

Figure 7. Microphotographs of samples with different content of clay minerals of the Da'anzhai Member. (a) Shell limestone with a significant number of clay minerals in the non-reservoir intervals (pointed by red arrow), plane-polarized light, the P-wave velocity is 4842 m s^{-1} and the S-wave velocity is 2737 m s^{-1} (Well PL10, 1981.57 m). (b) Shell limestone with no clay mineral in the reservoir intervals, plane-polarized light, the P-wave velocity is 5809 m s^{-1} and the S-wave velocity is 3095 m s^{-1} (Well PL10, 2034.93 m).

contains self-generated and self-reservoir oil and gas. Furthermore, Dayi and Dasan submembers are dominated by the argillaceous shell limestone and shell limestone, which provide reservoir space for oil and gas generated from the Dayisan submember; they mainly contain near-source accumulation oil and gas. The Da'anzhai Member reservoirs are characterized by <2% porosity and <0.1 mD permeability (Huang *et al.* 2018, Su *et al.* 2020). The main space types of reservoirs are micro-pores, fractures and dissolution pores (Zhu *et al.* 2022). Therefore, the Da'anzhai Member reservoirs are tight with a small pore throat radius, diverse pore structure and firm heterogeneity (Gan *et al.* 2009).

3. Materials and methods

This study conducted ultrasonic pulse-transmission and triaxial rock compression experiments to clarify the petrophysical characteristics of the Da'anzhai Member reservoirs and select sensitive parameters for reservoir identification. The 23 experimental samples come from five coring wells (PL10, PL111, PL15, LQ2 and LQ104 seen in figure 1). The sampling strata are the Da'anzhai Member, including 17 samples in the reservoir intervals and six samples in the non-reservoir intervals (Table 1). Figure 2 shows the photos of standard samples. The leftover samples are used for optical thin-section analysis to characterize the mineral and pore features.

The densities of the samples were determined by the weighing method, taking the average of three tests. Three ultrasonic pulse-transmission experiments using the CTS-8077PR pulse generator determined the acoustic velocities; the dominant frequency of ultrasonic transducer is 0.5 MHz. Young's moduli and Poisson's ratios were determined by a single triaxial rock compression experiment using

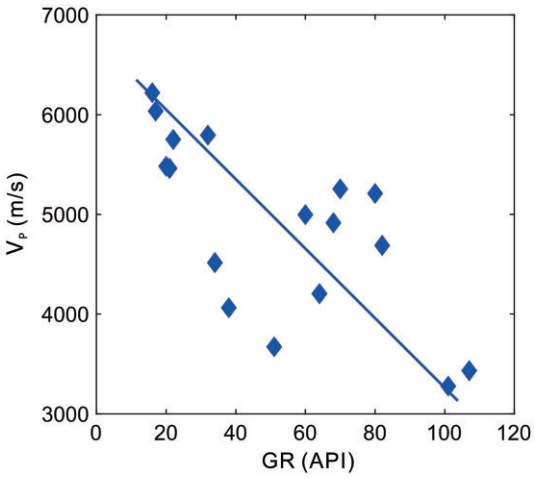

Figure 8. This figure shows the relationship between P-wave velocities (V_p) and gamma-ray logging values (GR) of the Da'anzhai Member reservoirs. As the gamma values decrease, the P-wave velocities gradually increase.

Tektronix DPO3012 digital phosphor oscilloscope. All parameters were determined under normal atmospheric temperature and pressure. The average error ranges between 1.36 and 2.53%, and the maximum error is 13.5%.

4. Results

4.1. Acoustic velocity

Figure 3 shows the results of the ultrasonic pulse-transmission experiments. The P-wave velocities (V_p) range between 1500 and 3000 m s^{-1} (figure 3a), which is the same as the P-wave velocities of the well logging interpretation (figure 3b). It shows that the higher formation temperature and pressure in the ground make the P-wave velocity obtained by logging in good agreement with that obtained in the laboratory, which provides some evidence for the laboratory data to better reflect the subsurface conditions (Wang *et al.* 2021; Wei *et al.* 2021; Liu *et al.* 2022). The S-wave velocities (V_s) range between 1500 and 2100 m s^{-1} (figure 3c); the V_p/V_s ratios (V_p/V_s) range between 0.7 and 0.9 (figure 3d), consistent with the characteristics of acoustic velocity in the tight limestone.

Figure 4 parts a–c show the statistical results of the acoustic velocity tests. In the reservoir intervals, P-wave velocities mainly range between 4500 and 5500 m s^{-1}, and the average value is 5127 m s^{-1}; S-wave velocities mainly range between 2500 and 3100 m s^{-1}, and the average value is 2817 m s^{-1}s; V_p/V_s ratios mainly range between 1.7 and 1.9, and the average value is 1.8224. In the non-reservoir intervals, P-wave velocities mainly range between 4500 and 5000 m s^{-1}, and the average value is 4680 m s^{-1}, while the S-wave velocities mainly range between 2500 and 2800 m s^{-1}, and the average value is 2695 m s^{-1}. The V_p/V_s ratios mainly range between 1.7 and 1.8, with an average value of 1.7368.

The results show that the distribution range of the acoustic velocities in the reservoir intervals overlaps severely with that of the non-reservoir intervals and shows high-value characteristics.

4.2. Elastic modulus

Figure 5 shows the results of triaxial compression experiments. Young's moduli (E) mainly range between 25 and 45 GPa (figure 5a); Poisson's ratios (ν) mainly range between 0.2 and 0.29 (figure 5b), consistent with the elastic characteristics of the tight limestone.

Figure 6 parts a–c show the results of the elastic moduli tests. In the reservoir intervals, Young's moduli mainly range between 25 and 55 GPa, with an average value of 40 GPa. Poisson's ratios mainly range between 0.11 and 0.29, with an average value of 0.2115. In the non-reservoir intervals, Young's moduli mainly range between 25 and 45 GPa, with an average value of 32 GPa. Poisson's ratios mainly range between 0.29 and 0.38, with an average value of 0.3433.

The analysis shows Young's moduli of the reservoir intervals present high-value characteristics and Poisson's ratios present low value characteristics. Young's moduli overlap severely in the reservoir and the non-reservoir intervals, but Poisson's ratios have apparent segmentation.

5. Discussion

Under actual geological conditions, various factors often influence the petrophysical properties of reservoirs. For example, fractures can significantly reduce acoustic velocity, clay minerals may reduce the V_p/V_s ratio, and rock pore structure and external hydrocarbon charging influence permeability, density and resistivity (Abdel-Fattah 2015; Kleipool *et al.* 2015; Lai *et al.* 2017, Liu & Ostadhassan 2017). These factors can be attributed to sedimentation, diagenesis, tectonism and resulting petrophysical characteristics of the reservoirs (Li *et al.* 2020; Xu *et al.* 2020; Zhu *et al.* 2022). In this study, we used thin sections, well logging interpretations and petrophysical experiments to analyse the main factors controlling the petrophysical characteristics and clarify the influencing mechanisms.

5.1. The influence of clay content on acoustic velocity

The clay content mainly influences the acoustic velocity. Through observations of thin sections, the micrographs of the reservoir and non-reservoir intervals of the Da'anzhai Member are shown in figure 7a and b, indicating that clay minerals cause a 967 m s^{-1} drop in P-wave velocity and a 358 m s^{-1} drop in S-wave velocity. Figure 8 shows the

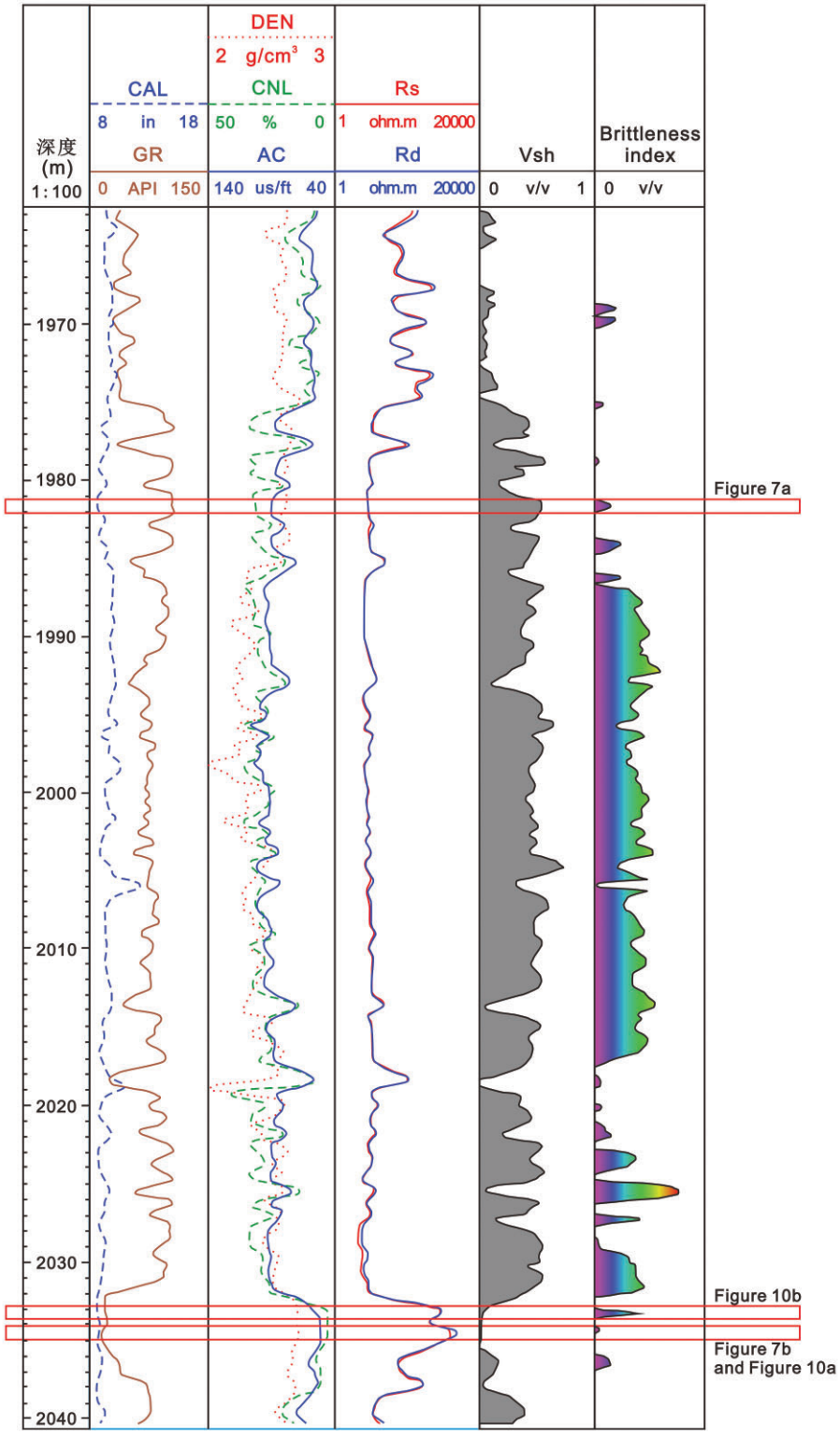

Figure 9. The reservoir parameters interpretation diagram of Da'anzhai member in Central Sichuan Basin (Modified from He *et al.* 2021)

relationship between the gamma-ray logging values and the P-wave velocities through well logging interpretation. As the gamma values decrease, the P-wave velocities gradually increase. The low clay content in the reservoir intervals is the primary reason for the characteristic of high acoustic velocity. Figure 9 shows the relationship between clay content and acoustic velocity. At the depth of the sampling point in figure 7a, the high clay content (V_{sh} curve) corresponds to

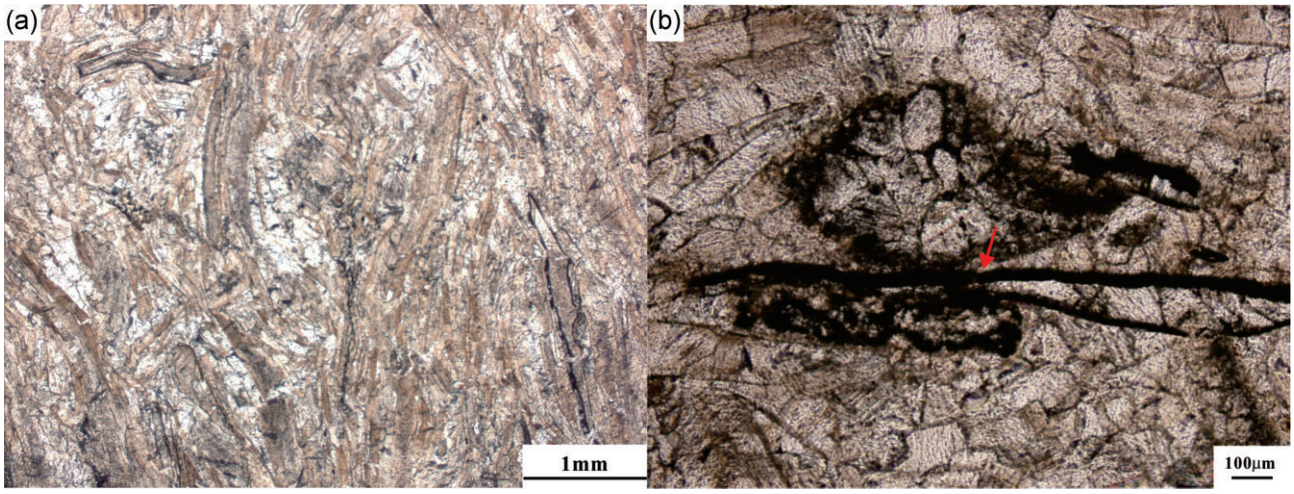

Figure 10. Microphotographs of samples with different degrees of fracture development in the Da'anzhai Member. (a) Shell limestone with few fractures in the reservoir intervals, plane-polarized light, the P-wave velocity is 5809 m s^{-1} and the S-wave velocity is 3095 m s^{-1} (Well PL10, 2034.93 m). (b) Shell limestone with large fractures and pores in the reservoir intervals (pointed by red arrow), plane-polarized light, the P-wave velocity is 4660 m s^{-1} and the S-wave velocity is 2685 m s^{-1} (Well PL10, 2033.33 m).

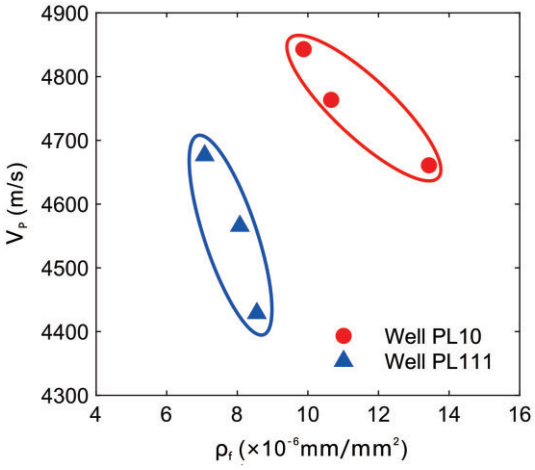

Figure 11. This figure shows relationship between P-wave velocity (V_p) and fracture density (ρ_f) in the Da'anzhai Member reservoirs. The P-wave velocity gradually decreases as the fracture density increases.

the low acoustic velocity (AC curve), whereas it is opposite at the depth of the sampling point in figure 7b, which shows the same laws as the laboratory results.

5.2. *The influence of fractures and laminae on acoustic velocity*

Rock fractures are the primary influence on acoustic velocity. Figure 10 parts a and b show the micrographs of the core samples with different degrees of fracture development in the reservoir intervals; fractures cause a 967 m s^{-1} drop in P-wave velocity and an approximately 410 m s^{-1} drop in S-wave velocity. Figure 11 shows the relationship between the fracture density and the P-wave velocity. The fracture density is obtained through calculation and correction based on cores of well PL10 and PL111. The P-wave velocity gradually decreases as the fracture density increases. Figure 9 shows the relationship between fracture development and acoustic velocity. The brittleness index curve reflects the fracture development. The higher the brittleness, the more fractures develop (Kahraman & Altindag 2004; Ba *et al.* 2021; Forbes Inskip & Meredith 2021). At the depth of the sampling point in figure 10a, the low brittleness index curve corresponds to the high acoustic velocity (AC curve), whereas it is opposite at the depth of the sampling point in figure 10b, which shows the same laws as the laboratory results.

Rock laminae can promote the formation of bedding fractures (Liu *et al.* 2020), so there is a specific concomitant relationship between the laminae and the fractures (Liu *et al.* 2017). Therefore, the laminae also influence acoustic velocity. Figure 12 parts a and b show micrographs of the core samples with different degrees of laminae development in the reservoir intervals. The laminae cause a 643 m s^{-1} drop in P-wave velocity and a 243 m s^{-1} drop in S-wave velocity.

The high-quality reservoirs with large fractures and laminae lead to a partly decline in acoustic velocity and therefore show relatively low value under the background of high acoustic velocity caused by low clay content.

5.3. *Optimization of reservoir identification parameters*

Reservoir identification by geophysical methods mainly depends on the differences in petrophysical properties. The selection of identification parameters involves finding the most distinct petrophysical parameters and determining the

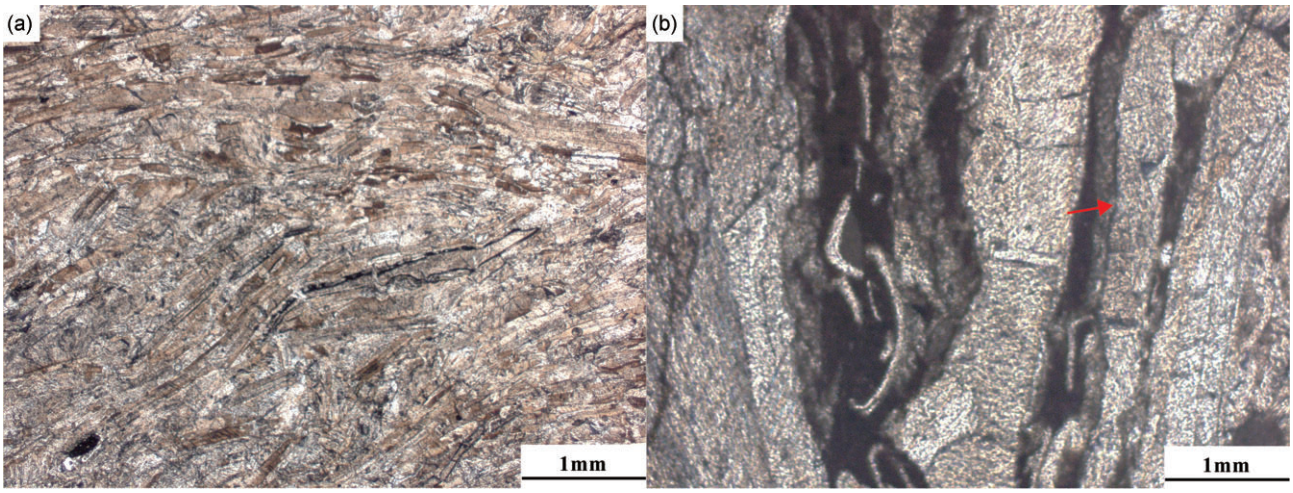

Figure 12. Microphotographs of samples with different degrees of lamina development in the Da'anzhai Member. (a) Shell limestone with no lamina in the reservoir intervals, plane-polarized light, the P-wave velocity is 5809 m s^{-1} and the S-wave velocity is 3095 m s^{-1} (Well PL10, 2034.93 m). (b) Shell limestone with large laminae in the reservoir intervals (pointed by red arrow), plane-polarized light, the P-wave velocity is 5166 m s^{-1} and the S-wave velocity is 2852 m s^{-1} (Well PL10, 2033.13 m).

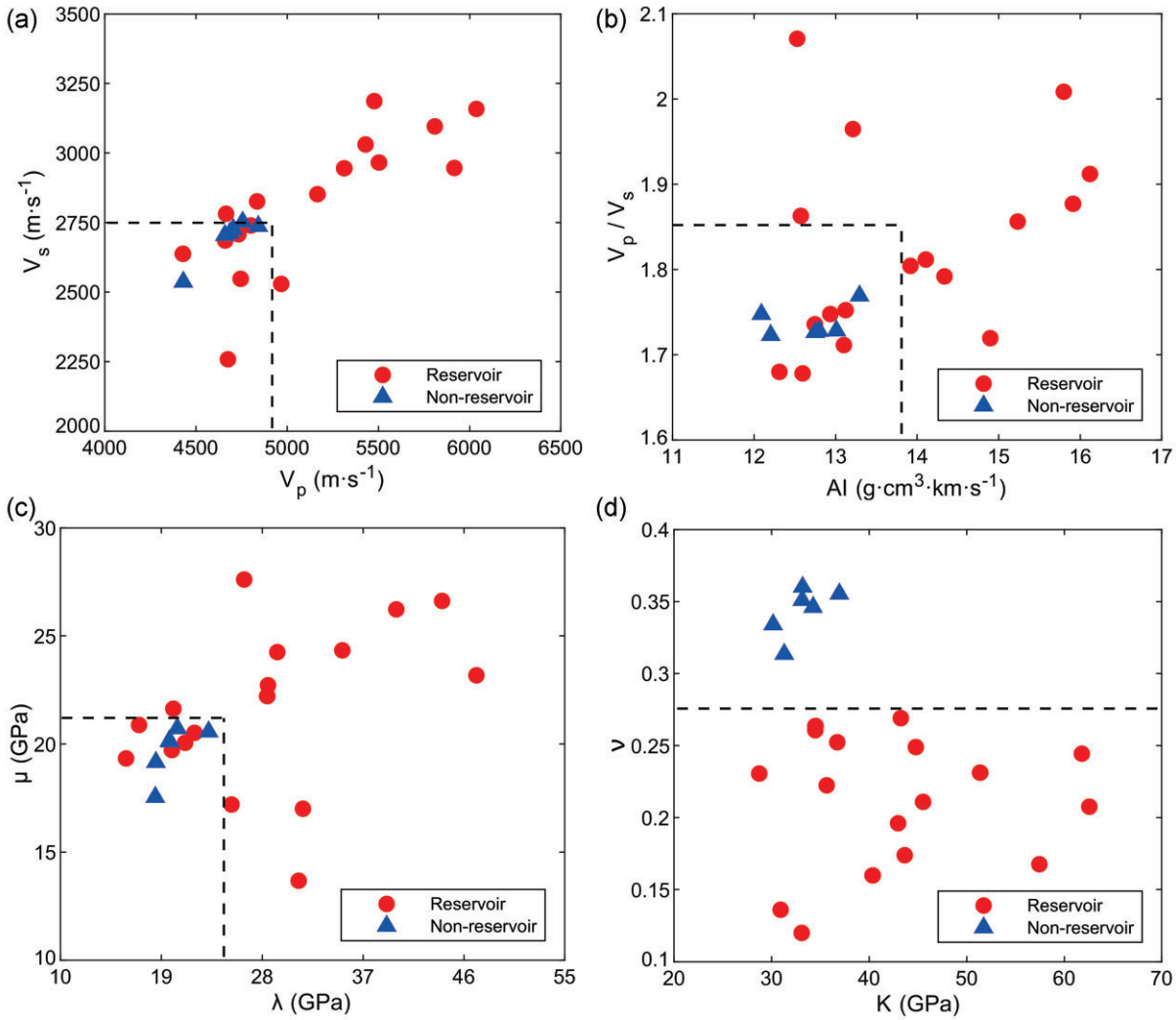

Figure 13. The cross plots of four groups of reservoir identification parameters. (a) P-wave velocities (V_p) and S-wave velocities (V_s). (b) Wave impedances (AI) and V_p/V_s ratios. (c) Lame constants (λ) and shear moduli (μ) and (d) Young's moduli (K) and Poisson's ratios (ν) in the reservoir and non-reservoir intervals.

threshold value to establish the criteria for reservoir identification (Singha & Chatterjee 2017; Mondal *et al.* 2018; Das *et al.* 2019). There have been numerous mature studies on the identification parameters of reservoirs with different lithologies, such as sandstone, limestone, dolomite, shale and volcanic rock (Fournier *et al.* 2018; Noorian *et al.* 2020; Li *et al.* 2021; Mondal *et al.* 2021; Jiang *et al.* 2022). However, the identification parameters for continental shale oil reservoirs of the Da'anzhai Member are still unclear. Therefore, based on the previous analysis of petrophysical characteristics, we further calculate elastic and wave resistance parameters and use the cross plot method to select sensitive parameters for reservoir identification. The bulk moduli, shear moduli, Lame constant and wave impedance can be calculated from the acoustic velocity and density using equations (1)–(4), respectively.

$$K = \rho\left(V_P^2 - 4V_S^2/3\right), \tag{1}$$

$$\mu = \rho V_S^2, \tag{2}$$

$$\lambda = \rho\left(V_P^2 - 2V_S^2\right), \tag{3}$$

$$AI = \rho V_P. \tag{4}$$

The four groups of parameters with a significant effect on reservoir identification are obtained (figure 13). The combination of P-wave velocity (V_p) and S-wave velocity (V_s), P-wave impedance (AI) and V_p/V_s ratio (V_p/V_s), Lame constant (λ) and shear modulus (μ) only partially identify the reservoirs; in comparison, the combination of Young's modulus (E) and Poisson's ratio (ν) can fully identify the reservoir intervals. Further analysis shows the cross plot of P- and S-wave velocities. When P-wave velocity is >4967 m s^{-1} and S-wave velocity is >2781 m s^{-1}, 11 reservoir points can be identified (figure 13a). The same conclusion is obtained in the cross plot of P-wave impedances and the V_p/V_s ratios when the P-wave impedance is >13.319 g · cm^3 · km · s^{-1}, and the V_p/V_s ratio is >1.792 (figure 13b). In the cross plot of the Lame constants and shear moduli, 12 reservoir points can be identified when the Lame constant is >25.277 GPa and the shear modulus is >20.72 GPa (figure 13c). Finally, in the cross plot of bulk moduli and Poisson's ratios, all the reservoir points can be identified when Poisson's ratio is <0.269 (figure 13d).

In conclusion, Poisson's ratio ($\nu < 0.269$) should be used as the main sensitive parameter for reservoir identification. In addition, the combination of the Lame constant and shear modulus ($\lambda > 25.277$ and $\mu > 20.72$ GPa), the combination of P- and S-wave velocity ($V_p > 4967$ and $V_s > 2781$ m s^{-1}) and the combination of P-wave impedance, and V_p/V_s ratio (AI > 13.319 g · cm^3 · km · s^{-1} and $V_p/V_s > 1.792$) can also provide references for reservoir identification.

6. Conclusions

(i) The Jurassic Da'anzhai Member reservoirs in the Central Sichuan Basin show the characteristics of high acoustic velocities, V_p/V_s ratios and Young's moduli and low Poisson's ratios.

(ii) Clay content, fractures and laminae mainly influence the petrophysical characteristics of the Da'anzhai Member reservoirs. The low clay content in reservoirs causes a general characteristic of high acoustic velocity. However, the fractures and laminae of high-quality reservoirs lead to a large decline in acoustic velocity. Therefore, the relatively low value under the background of high acoustic velocity can be used as the criterion for identifying high-quality continental shale oil reservoirs.

(iii) Poisson's ratio is the most sensitive identification parameter. The reservoirs can be fully identified when Poisson's ratio is less than 0.269. In addition, the combination of the Lame constant and shear modulus ($\lambda >$ 25.277 and $\mu > 20.72$ GPa), the combination of P- and S-wave velocity ($V_p > 4967$ and $V_s > 2781$ m s^{-1}) and the combination of wave impedance and V_p/V_s ratio (AI > 13.319 g · cm^3 · km · s^{-1} and $V_p/V_s > 1.792$) can also provide references for reservoir identification.

Acknowledgements

This work is supported by the National Natural Science Foundation of China (grant no. U1663203 and grant no. 42104107).

Conflict of interest statement. None declared.

References

Abdel-Fattah, M.I., 2015. Impact of depositional environment on petrophysical reservoir characteristics in Obaiyed Field, Western Desert, Egypt, *Arabian Journal of Geosciences*, **8**, 9301–9314.

Aleardi, M., 2018. Estimating petrophysical reservoir properties through extended elastic impedance inversion: applications to off-shore and on-shore reflection seismic data, *Journal of Geophysics and Engineering*, **15**, 2079–2090.

Ba, J., Hu, P., Tan, W.H., Muller, T.M.M. & Fu, L.Y., 2021. Brittle mineral prediction based on rock-physics modelling for tight oil reservoir rocks, *Journal of Geophysics and Engineering*, **18**, 970–983.

Chen, S.J. et al., 2015. Controlling factors of Jurassic Da'anzhai Member tight oil accumulation and high production in central Sichuan Basin, SW China, *Petroleum Exploration and Development*, **42**, 206–214.

Das, P.S., Chatterjee, R., Dasgupta, S., Das, R., Bakshi, D. & Gupta, M., 2019. Quantification and spatial distribution of pore-filling materials through constrained rock physics template and fluid response modelling in Paleogene clastic reservoir from Cauvery basin, India, *Geophysical Prospecting*, **67**, 150–166.

Ding, W.L., Dai, P., Zhu, D.W., Zhang, Y.Q., He, J.H., Li, A. & Wang, R.Y., 2016. Fractures in continental shale reservoirs: a case study of the Upper Triassic strata in the SE Ordos Basin, Central China, *Geological Magazine*, **153**, 663–680.

Forbes Inskip, N.D. & Meredith, P.G., 2021. Fracture properties of Nash point limestone and implications for fracturing of layered carbonate sequences, *Rock Mechanics and Rock Engineering*, **54**, 5155–5166.

Fournier, F., Pellerin, M., Villeneuve, Q., Teillet, T., Hong, F., Poli, E., Borgomano, J., Léonide, P. & Hairabian, A., 2018. The equivalent pore aspect ratio as a tool for pore type prediction in carbonate reservoirs, *AAPG Bulletin*, **102**, 1343–1377.

Gan, Q., Xu, D., Tang, J. & Wang, Y., 2009. Seismic resolution enhancement for tight-sand gas reservoir characterization, *Journal of Geophysics and Engineering*, **6**, 21–28.

Gao, Y.L., Liu, H.Q., Pu, C., Tang, H.Y., Yang, K. & Dong, X.H., 2021. Impact of geomechanical heterogeneity on multiple hydraulic fracture propagation, *Journal of Geophysics and Engineering*, **18**, 954–969.

Gong, L., Fu, X.F., Wang, Z.S., Gao, S., Jabbari, H., Yue, W. & Liu, B., 2019. A new approach for characterization and prediction of natural fracture occurrence in tight-oil sandstones with intense anisotropy, *AAPG Bulletin*, **103**, 1383–1400.

Gong, L. et al., 2021a. Quantitative Prediction of Natural Fractures in Shale Oil Reservoirs, *Geofluids*, **2021**, 5571855.

Gong, L., Wang, J., Gao, S., Fu, X.F., Liu, B., Miao, F.B., Zhou, X.P. & Meng, Q.K., 2021b. Characterization, controlling factors and evolution of fracture effectiveness in shale oil reservoirs, *Journal of Petroleum Science and Engineering*, **203**, 108655.

He, X.Q., Huang, D., Zhao, A.L. & Li, Y.C., 2021. Well-logging evaluation index system of shale oil and gas reservoir of Da'anzhai member in central Sichuan Basin, *Lithologic Reservoirs*, **33**, 129–137.

Huang, D., Duan, Y., Yang, G., Yan, W.P., Wei, T.Q., Zou, J., Wang, W. & Li, Y.C., 2018. Controlling effect of source-reservoir configuration model on tight oil enrichment in freshwater lacustrine sedimentary area: a case study of the Jurassic Da'anzhai Member in Sichuan Basin, *Acta Petrolei Sinica*, **39**, 518–527 (in Chinese with English abstract).

Jiang, Z.R., Qi, Q.M., Jiang, X.D., Meng, J.K. & Wang, X. J., 2022. An efficient rock physics scheme for estimating crack density and fluid saturation of shale gas reservoir, *Frontiers in Earth Science*, **9**, 829244.

Kahraman, S.A. & Altindag, R., 2004. A brittleness index to estimate fracture toughness, *International Journal of Rock Mechanics and Mining Sciences*, **41**, 343–348.

Karimpouli, S., Hassani, H., Nabi-Bidhendi, M., Khoshdel, H. & Malehmir, A., 2013. Application of probabilistic facies prediction and estimation of rock physics parameters in a carbonate reservoir from Iran, *Journal of Geophysics and Engineering*, **10**, 015008.

Kleipool, L.M., Reijmer, J.J.G., Badenas, B. & Aurell, M., 2015. Variations in petrophysical properties along a mixed siliciclastic carbonate ramp (Upper Jurassic, Ricla, NE Spain), *Marine and Petroleum Geology*, **68**, 158–177.

Lai, Q., Xie, B., Wu, Y.Y., Huang, K., Liu, X.G., Jin, Y., Luo, W. & Liang, T., 2017. Petrophysical characteristics and logging evaluation of asphaltene carbonate reservoirs: a case study of the Cambrian Longwangmiao Formation in Anyue gas field, Sichuan Basin, SW China, *Petroleum Exploration and Development*, **44**, 941–947.

Li, B., Wang, X.Z., Liu, H.Q., Wang, Y.J., Tian, J., Huo, F. & Gao, Z.L., 2020. Tight carbonate microstructure and its controls: a case study of lower Jurassic Da'anzhai Member, Central Sichuan Basin, *Acta Geologica Sinica-English Edition*, **94**, 305–321.

Li, H.T., Deng, S.G., Wang, Y.X. & He, X.Q., 2021. Study on identification method of gas-bearing carbonate reservoirs based on joint acoustic-resistivity experiments - an example from the Sichuan Basin of China, *Exploration Geophysics*, **52**, 475–483.

Li, W.K., Wang, J., Li, J.S., Liu, X.H., Chen, K. & He, Q.L., 2018. Characteristics and origin of the Sinian-Permian fault system and its controls on the formation of paleo-carbonate reservoirs: a case study from Central Paleo-Uplift, Sichuan Basin, China, *Interpretation-a Journal of Subsurface Characterization*, **6**, T191–T208.

Li, Y.Q. & He, D.F., 2014. Evolution of tectonic-depositional environment and prototype basins of the Early Jurassic in Sichuan Basin and adjacent areas, *Acta Petrolei Sinica*, **35**, 219–232 (in Chinese with English abstract).

Li, Y.Q., He, D.F., Chen, L.B., Mei, Q.H., Li, C.X. & Zhang, L., 2016. Cretaceous sedimentary basins in Sichuan, SW China: restoration of tectonic and depositional environments, *Cretaceous Research*, **57**, 50–65.

Liu, B., Wang, S., Ke, X., Fu, X.F., Liu, X.Z., Bai, Y.F. & Pan, Z.J., 2020. Mechanical characteristics and factors controlling brittleness of organic-rich continental shales, *Journal of Petroleum Science and Engineering*, **194**, 107646.

Liu, G.Q., 2021. Challenges and countermeasures of log evaluation in unconventional petroleum exploration and development, *Petroleum Exploration and Development*, **48**, 1033–1047.

Liu, H.M., Zhang, S., Song, G.Q., Zhang, S.P., Hao, X.F., Xie, Z.H., Xu, N.N. & Liu, P., 2017. A discussion on the origin of shale reservoir interlaminar fractures in the Shahejie Formation of Paleogene, Dongying depression, *Journal of Earth Science*, **28**, 1064–1077.

Liu, K.Q. & Ostadhassan, M., 2017. Microstructural and geomechanical analysis of Bakken shale at nanoscale, *Journal of Petroleum Science and Engineering*, **153**, 133–144.

Liu, W., Zhang, G.L., Cao, J.X., Zhang, J.J. & Yu, G., 2019. Combined petrophysics and 3D seismic attributes to predict shale reservoirs favourable areas, *Journal of Geophysics and Engineering*, **16**, 974–991.

Liu, Z.C., Peng, R., Li, X., Du, X., Zhu, Z., Li, X. & Li, H., 2022. Wave velocity in shale in the Wufeng-Longmaxi formation in Sichuan Basin, *Journal of Geophysics and Engineering*, **19**, 283–294.

Liu, Z.J. et al., 2021. Types and quantitative characterization of microfractures in the continental shale of the Da'anzhai Member of the Ziliujing Formation in Northeast Sichuan, China, *Minerals*, **11**, 870.

Mondal, S., Chatterjee, R. & Chakraborty, S., 2021. An integrated approach for reservoir characterisation in deep-water Krishna-Godavari basin, India: a case study, *Journal of Geophysics and Engineering*, **18**, 134–144.

Mondal, S., Yadav, A. & Chatterjee, R., 2018. Integration of rock physical signatures with depositional environments: a case study from East Coast of India, *Journal of Applied Geophysics*, **148**, 256–264.

Noorian, Y., Moussavi-Harami, R., Mahboubi, A., Kadkhodaie, A. & Omidpour, A., 2020. Assessment of heterogeneities of the Asmari reservoir along the Bibi Hakimeh anticline using petrophysical and sedimentological attributes: southeast of Dezful Embayment, SW Iran, *Journal of Petroleum Science and Engineering*, **193**, 107390.

Pang, Z.L. et al., 2018. Reservoir micro structure of Da'anzhai Member of Jurassic and its petroleum significance in Central Sichuan Basin, SW China, *Petroleum Exploration and Development*, **45**, 68–78.

Pang, Z.L. et al., 2020. Evaluation methods of profitable tight oil reservoir of Lacustrine Coquina: a case study of Da'anzhai Member of Jurassic in the Sichuan Basin, *Acta Geologica Sinica-English Edition*, **94**, 418–429.

Peng, C.Z., Peng, J., Chen, Y.H. & Zhang, H.R., 2014. Seismic prediction of sweet spots in the Da'anzhai Shale Play, Yuanba area, Sichuan Basin, *Natural Gas Industry*, **34**, 42–47 (in Chinese with English abstract).

Singha, D.K. & Chatterjee, R., 2017. Rock physics modeling in sand reservoir through well log analysis, Krishna-Godavari basin, India, *Geomechanics and Engineering*, **13**, 99–117.

Su, J., Tian, Z.P., Shen, Y.C., Liu, B., Xu, Q.L. & Wang, Y.J., 2020. Differential diagenetic evolution and hydrocarbon charging of the tight limestone reservoir of the Da'anzhai Member in the central Sichuan Basin, China, *Interpretation-a Journal of Subsurface Characterization*, **8**, T1007–T1022.

Sun, J., Chi, P., Cheng, Z., Yang, L., Yan, W. & Cui, L., 2021. A novel saturation calculation model of fractured-vuggy carbonate reservoir via multiscale pore networks: a case study from Sichuan Basin, China, *Journal of Geophysics and Engineering*, **18**, 85–97.

Tian, J., Liu, H.Q., Wang, L., Sima, L.Q., Liu, S.Q. & Liu, X.J., 2021. Identification of fractures in tight-oil reservoirs: a case study of the Da'anzhai member in the central Sichuan Basin, SW China, *Scientific Reports*, **11**, 23846.

Tian, Z.P., Song, X.M., Wang, Y.J., Ran, Q.Q., Liu, B., Xu, Q.L. & Li, Y., 2017. Classification of lacustrine tight limestone considering matrix pores or fractures: a case study of Da'anzhai Member of Jurassic Ziliujing Formation in central Sichuan Basin, SW China, *Petroleum Exploration and Development*, **44**, 234–246.

Wang, X., He, S., Guo, X.W., Zhang, B.Q. & Chen, X.H., 2018. The resource evaluation of Jurassic shale in North Fuling area, eastern Sichuan Basin, China, *Energy & Fuels*, **32**, 1213–1222.

Wang, Z.Z., Njiekak, G., Schmitt, D.R. & Wang, R.H., 2021. Empirical rock physics relationships on carbonate dry-frame elastic properties, *Petroleum Science*, **18**, 783–806.

Wei, Y.J., Ba, J., Carcione, J.M., Fu, L.Y., Pang, M.Q. & Qi, H., 2021. Temperature, differential pressure, and porosity inversion for ultradeep carbonate reservoirs based on 3D rock-physics templates, *Geophysics*, **86**, 77–89.

Xu, H.L., Wei, G.Q., Jia, C.Z., Yang, W., Zhou, T.W., Xie, W.R., Li, C.X. & Luo, B.W., 2012. Tectonic evolution of the Leshan-Longnusi paleouplift and its control on gas accumulation in the Sinian strata, Sichuan Basin, *Petroleum Exploration and Development*, **39**, 406–416.

Xu, Q.L., Hao, F., Ma, Y.S., Liu, B. & Song, X.M., 2020. Effects of the matrix on the oil production of supertight limestone in a lacustrine mixed sedimentary environment: the case of the Jurassic Da'anzhai member in the central Sichuan Basin, China, *Marine and Petroleum Geology*, **121**, 104583.

Xu, Q.L., Liu, B., Ma, Y.S., Song, X.M., Wang, Y.J. & Chen, Z.X., 2017. Geological and geochemical characterization of lacustrine shale: a case study of the Jurassic Da'anzhai member shale in the central Sichuan Basin, southwest China, *Journal of Natural Gas Science and Engineering*, **47**, 124–139.

Xu, Q.L. et al., 2018. Fractal characteristics of lacustrine tight carbonate nanoscale reservoirs, *Energy & Fuels*, **32**, 107–118.

Xu, Q.L., Ma, Y.S., Liu, B., Song, X.M., Su, J. & Chen, Z.X., 2019. Characteristics and control mechanism of nanoscale pores in lacustrine tight carbonates: examples from the Jurassic Da'anzhai Member in the central Sichuan Basin, China, *Journal of Asian Earth Sciences*, **178**, 156–172.

Yang, G., Huang, D., Huang, P.H., Yang, W.P., Yang, T.Q., Dai, H.M. & Lin, J.P., 2017. Control factors of high and stable production of Jurassic Da'anzhai Member tight oil in central Sichuan Basin, SW China, *Petroleum Exploration and Development*, **44**, 866–875.

Yang, Y.M. et al., 2016. New research progress of Jurassic tight oil in central Sichuan Basin, SW China, *Petroleum Exploration and Development*, **43**, 954–964.

Zeng, L.B., 2010. Microfracturing in the Upper Triassic Sichuan Basin tight-gas sandstones: tectonic, overpressure, and diagenetic origins, *AAPG Bulletin*, **94**, 1811–1825.

Zeng, L.B., Gong, L, Guan, C., Zhang, B.J., Wang, Q.Q., Zeng, Q. & Lyu, W.Y., 2022. Natural fractures and their contribution to tight gas conglomerate reservoirs: a case study in the northwestern Sichuan Basin, China, *Journal of Petroleum Science and Engineering*, **210**, 110028.

Zeng, L.B., Lyu, W.Y., Li, J., Zhu, L.F., Weng, J.Q., Yue, F. & Zu, K.W., 2016. Natural fractures and their influence on shale gas enrichment in Sichuan Basin, China, *Journal of Natural Gas Science and Engineering*, **30**, 1–9.

Zeng, L.B., Wang, Z.G., Xiao, S.R. & Zhang, G.B., 2009. The origin and geological significance of low dip-angle fractures in the thrust zones of the western basins of China, *Acta Petrolei Sinica*, **30**, 56–60 (in Chinese with English abstract).

Zhang, R. & Tang, L.X., 2022. Oil-bearing evaluation of different lithofacies in Da'anzhai Member, Central Sichuan Basin: implications for shale oil development, *Petroleum Science and Technology*, **8**, 1–15.

Zhu, Y.X., Li, Z.Z., Zeng, L.B., Liu, Z.Y. & Wang, X.Y., 2022. Diagenesis and its impact on the reservoir quality of continental shales: a case study of the Lower Jurassic Da'anzhai Member of the Ziliujing Formation in the Sichuan Basin, China, *Geofluids*, **2022**, 5942370.